Journal of Hazardous Materials 458 (2023) 131966

Contents lists available at ScienceDirect

Journal of Hazardous Materials

journal homepage: www.elsevier.com/locate/jhazmat

Viral inactivation using microwave-enhanced membrane filtration

Fangzhou Liu [a], Bruce Rittmann [b], Saachi Kuthari [a,c], Wen Zhang [a,*]

[a] John A. Reif, Jr. Department of Civil and Environmental Engineering, New Jersey Institute of Technology, 323 Martin Luther King Blvd., Newark, NJ, USA
[b] Biodesign Swette Center for Environmental Biotechnology, Arizona State University, Tempe, AZ, USA
[c] Millburn High School, Short Hills, NJ, USA

HIGHLIGHTS

- Microwave catalytic membrane filtration achieved effective viral inactivation.
- Microwave irradiation intensity and exposure time affects viral inactivation performances.
- Generation of radicals were confirmed by EPR measurement and radical scavenging experiments.
- The MS2 inactivation mechanisms under microwave heating and conventional heating are different.
- COMSOL Multiphysics simulation unresolved microwave penetration and heat distribution.

GRAPHICAL ABSTRACT

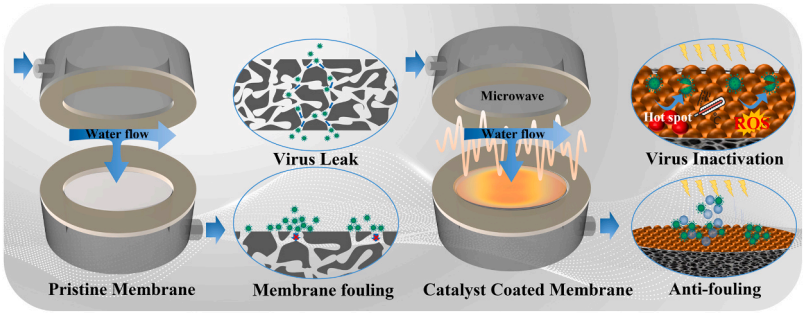

ARTICLE INFO

Editor: Meiping Tong

Keywords:
Microwave disinfection
Microwave catalysis
Waterborne virus
Bacteriophage MS2

ABSTRACT

Pathogenic viruses (e.g., Enteroviruses, Noroviruses, Rotaviruses, and Adenovirus) present in wastewater, even at low concentrations, can cause serious waterborne diseases. Improving water treatment to enhance viral removal is of paramount significance, especially given the COVID-19 pandemic. This study incorporated microwave-enabled catalysis into membrane filtration and evaluated viral removal using a model bacteriophage (MS2) as a surrogate. Microwave irradiation effectively penetrated the PTFE membrane module and enabled surface oxidation reactions on the membrane-coated catalysts (i.e., $BiFeO_3$), which thus elicited strong germicidal effects via local heating and radical formation as reported previously. A log removal of 2.6 was achieved for MS2 within a contact time as low as 20 s using 125-W microwave irradiation with the initial MS2 concentration of 10^5 PFU•mL^{-1}. By contrast, almost no inactivation could be achieved without microwave irradiation. COMSOL simulation indicates that the catalyst surface could be heated up to 305 °C with 125-W microwave irradiation for 20 s and also analyzed microwave penetration into catalyst or water film layers. This research provides new insights to the antiviral mechanisms of this microwave-enabled catalytic membrane filtration.

1. Introduction

Due to their small sizes (e.g., 10–100 nm), low infectious doses, strong pathogenicity, and resistance to disinfectants, viruses pose acute health risks [1–3]. Effective viral removal and inactivation technologies are of paramount significance for mitigating microbial risks. Waterborne

* Corresponding author.
E-mail address: wen.zhang@njit.edu (W. Zhang).

https://doi.org/10.1016/j.jhazmat.2023.131966
Received 19 April 2023; Received in revised form 5 June 2023; Accepted 27 June 2023
Available online 30 June 2023
0304-3894/© 2023 Elsevier B.V. All rights reserved.

viruses could be inactivated by many chemical disinfectants in traditional disinfection [4]. For example, 0.5 mg•L^{-1} free chlorine, 2.2 mg•L^{-1} chlorine dioxide, and 1 mg•L^{-1} ozone were sufficient for the inactivation of a wide spectrum of viruses, including SARS-CoV, by damaging viral capsids, viral genomes, and surface proteins [5–7]. However, chemical disinfection may generate potentially mutagenic and carcinogenic disinfection byproducts (DBPs) [8,9]. Furthermore, some persistent viruses (e.g., adenovirus [10], endornaviruses [11], enterovirus [12], and norovirus [13]) may not be effectively removed or inactivated.

Physical separation, such as ultrafiltration (UF), nanofiltration (NF), and reverse osmosis (RO), effectively removes viruses via size exclusion [14], electrostatic repulsion [15], adsorption retention [16], or hydrophobic interactions [16]. For instance, NF with nominal pore sizes of 2–10 nm and RO achieved 4- to 6-log removals for bacteriophage (e.g., MS2) [17,18]. However, only about 2- to 3-log removal could be achieved by UF (pore size of 5–50 nm) for norovirus, adenovirus, and rotavirus [19,20]. Log removal was further reduced when the membrane's pore size was increased: e.g., 0.3–2.2 log removal for microfiltration with pore sizes of 100–10,000 nm [19].

Recently, chemically reactive or catalytic membrane technologies have proven increasingly effective for viral removal and inactivation by producing germicidal radicals via photocatalysis [4,21,22]and electrochemical oxidation [23,24]. For instance, a photocatalytic membrane coated with N-doped TiO_2 demonstrated 4.9 ± 0.1 log removal for MS2 in natural surface water by solar UV–visible light [25]. In addition, a 6.7-log reduction of MS2 was achieved by an electrochemical membrane made with Ti_4O_7 using a current density of 10 mA•cm^{-2} [26]. Though these reactive membranes largely overcome the deficiency of removing ultra-small viruses, they still suffer from poor light penetration, membrane corrosion or fouling, and disinfection byproducts. For instance, photocatalytic membrane filtration is restricted to flat sheet membranes in order to permit light exposure to the catalysts. Electrocatalysts in electrochemical membrane filtration may undergo aging and passivation due to catalyst oxidation under application of high intensities of currents or voltages [27,28], which create localized changes of solution pH and radicals.

Microwave irradiation is widely used in food industries for surface sanitization [29–31], inactivates microorganisms by interfering with their ion channels and damaging their cell membrane via electroporation and localized heating [30]. Besides the thermal effects, microwaves can induce non-thermal degradation of biomolecules via radical formation. Catalyst-coated membranes also resist membrane fouling and achieve degradation of recalcitrant pollutants such as 1,4-dioxane and perfluorooctanoic acid (PFOA) via a microwave-Fenton-like reaction [32,33]. More importantly, microwaves can penetrate membrane modules and selectively activate catalysts on the membrane surfaces while not producing toxic byproducts. Up to now, the antiviral performance of this microwave catalytic membrane filtration has not been investigated.

This study employed a membrane coated with $BiFeO_3$ (BFO) as a microwave responsive catalyst, which demonstrates excellent capacity in microwave adsorption [34,35] and catalytic activity [32,36]. These properties permit effective evaluation of its the viral-removal performances and inactivation mechanisms. Bacteriophage MS2 (genus *Levivirus,* genogroup I) was the model virus, as it has many properties similar to common pathogenic viruses (e.g., a small size of 27 nm, negative surface charges [37], and hydrophobicity [38]). The log removal of MS2 in batch and continuous filtration modes was evaluated and compared with or without the catalyst coating and microwave irradiation. The effects of hydraulic retention time (HRT) and microwave irradiation time on the removal efficiency and system pressure were studied. The mechanisms of MS2 inactivation on the membrane/water interface were analyzed by measuring reactive oxygen species (ROS) and mapping the thermal distribution across the catalyst layer.

2. Materials and methods

2.1. $BiFeO_3$ (BFO) catalyst synthesis and preparation of catalyst-coated ceramic membranes

A microwave-assisted hydrothermal method was used to synthesize the powder form of the BFO catalyst. Briefly, $Bi(NO_3)_3{\cdot}5\ H_2O$ (1 mM) and $Fe(NO_3)_3{\cdot}9\ H_2O$ (1 mM) were mixed in a 1:1 in molar ratio. A NaOH solution (1 M) was then gradually added to the mixture with stirring for 15 min. Next, the solution was heated at 190 °C for 30 min in a microwave oven (300 W, 2.45 GHz). The black solid was separated by centrifugation (5000g for 20 min) and was washed at least three times with DI water and ethanol. Finally, the catalyst powder was vacuum dried for 12 h at 60 °C.

The catalyst particles were then spray-coated on a flat-sheet ceramic membrane (47N014, Sterlitech Corporation, US) that had a nominal pore size of 140 nm, a diameter of 4.6 cm, and an effective surface area of 17.34 cm^2. An optimal BFO-coating density (1.6 μg•cm^{-2}) was established in our previous study [33], which also reported the coating layer morphology, permeate flux, and the stability of the BFO-coated membranes. Figs. S1a-S1b in Supporting Information (SI) illustrate the major morphological changes before and after the surface coating of BFO catalysts. The catalyst-layer thickness was around 2 μm (Fig. S1c). The EDX spectra in Fig. S1d-S1e confirm the presence of oxygen, bismuth, and iron on the BFO-coated membrane.

2.2. Propagation and enumeration of MS2

Freeze-dried bacteriophage MS2 powder (ATCC 15597B1) was purchased from ATCC Company, USA. The revival and propagation of MS2 are described in detail in **Section S2**. Briefly, the standard double-layer agar method was applied for the enumeration of MS2 with Tryptic Soy Agar (BD Difco 236950, Cat.DF0369176), and the MS2 concentration was determined with the plaque-forming unit (PFU) [39]. Only the plates with 20–300 plaques were selected for counting. Moreover, all materials and glassware for the cultivation and propagation of MS2 were sterilized by autoclaving. All the tests were performed in triplicate.

2.3. Batch inactivation experiments

Batch experiments were first conducted to evaluate the MS2 inactivation in the BFO catalyst suspension. The MS2 suspension was added to the 1.5-mL sterilized microcentrifuge tubes (Thermo Scientific™ 90410) containing 1 mL of the 1X PBS solution to yield an initial concentration of ~10^5 PFU•mL^{-1}. The centrifuge tubes were then placed under the following conditions: (1) no treatment at room temperature as a negative control to determine the natural decay or inactivation of MS2 in PBS, (2) spiked with the BFO catalyst (0.2 g•L^{-1}) and storage at room temperature, (3) exposed to 125-W microwave irradiation (2.45 GHz) without the BFO catalysts, (4) exposed to the BFO catalyst and 125-W microwave irradiation (2.45 GHz), and (5) MS2 spiked into the pre-heated PBS at 35 ± 2 °C, 43 ± 2 °C, 59 ± 1 °C, and 70 ± 3 °C without exposure to microwave or catalyst to examine the heating effect on MS2 decay. To avoid possible artifacts, 0.99 mL PBS was pre-heated under the same microwave conditions (i.e., 30 s, 60 s and 120 s) to achieve the three solution temperatures, followed by immediate addition of 0.01 mL of the MS2 suspension. The log removal or reduction value (LRV) was computed by Eq. (1):

$$LRV = \log\left(\frac{N_t}{N_0}\right) \quad (1)$$

where N_t is the number of MS2 at treatment time t; and N_0 is the number of MS2 at time 0.

2.4. MS2 inactivation assay in continuous filtration experiments

As illustrated in Fig. 1, a dead-end filtration cell made of Teflon (PTFE) holding the catalyst-coated membrane was placed inside a commercial microwave (2.45 GHz, Panasonic Co., China). The synthetic wastewater (e.g., a MS2 suspension) was continuously pumped through the membrane cell by a peristaltic pump (UX-77921–75, Masterflex L/S, Cole-Parmer, USA) at different permeate fluxes. An IR Infrared Thermal Imaging Camera (Model HTI-19) was used to monitor the temperatures of the filtration cell and other parts (e.g., pipe, influent and effluent).

Before running any experiments, the filtration system was flushed with the sterile 1X PBS solution for 30 min to reach a stable permeate water flux and remove any contamination. The contributions from physical separation and the microwave-enabled viral inactivation or removal were evaluated by switching microwave irradiation "on" or "off". The MS2 concentrations in the feed and permeate samples were measured to calculate the LRV. Transmembrane pressure (TMP) and permeate temperature (near the permeate outlet) also were monitored during the filtration process. The morphology of phage particles before and after treatments was examined using transmission electron microscopy (TEM, JEOL JEM-F200) at 200 kV accelerated voltage; detailed methods are provided in SI.

To examine the stability of the coated membrane for MS2 inactivation under microwave irradiation, five consecutive filtration cycles (60 min per filtration cycle) were conducted to study potential membrane fouling and antimicrobial activity with an initial MS2 concentration of ~10^5 PFU•mL^{-1} and 5-min hydraulic cleaning (immersing the membrane in DI water and stirring at 200 rpm for 5 min). The transmembrane pressure (TMP) and LRV of MS2 were measured to indicate the membrane fouling and antimicrobial activity.

2.5. Detection of ROS

Typical ROS -hydroxyl radical (•OH) and superoxide radical (•O^{2-})- were detected as evidence for a non-thermal effect from the microwave catalytic reactions. Briefly, 4-hydroxy-TEMPO (Thermo Scientific™ Cat. AAA1249706) was used to scavenge •O^{2-} radicals due to its stability and rapid diffusion [40]. Mannitol (Thermo Scientific™ Cat. AAA1403030) was selected to quench •OH radicals instead of using tertiary butanol, which has a low-boiling point and thus could vaporize under high temperatures under microwave [41]. One mM TEMPOL and 0.5 M mannitol were spiked into the MS2 suspensions that also were mixed with different concentrations of BFO catalyst (0.05, 0.2 and 0.5 g•L^{-1}) and then irradiated by microwave for 60 s. The control experiments were conducted by spiking 1 mM TEMPOL and 0.5 M mannitol into the MS2 suspension (~10^5 PFU•mL^{-1}) for 60 s without microwave irradiation; they confirmed no evident changes in the LRVs (Fig. S2), suggesting a negligible germicidal effect of the selected scavengers on MS2 [42,43].

In addition, electron paramagnetic resonance (EPR) measurements were utilized to detect the presence of free radicals that might arise during BFO-catalyzed viral inactivation under microwave irradiation. A spin trapping method was employed to detect the occurrence of·OH and superoxide radicals (•O^{2-}) using 5,5-Dimethyl-1-pyrroline N-oxide

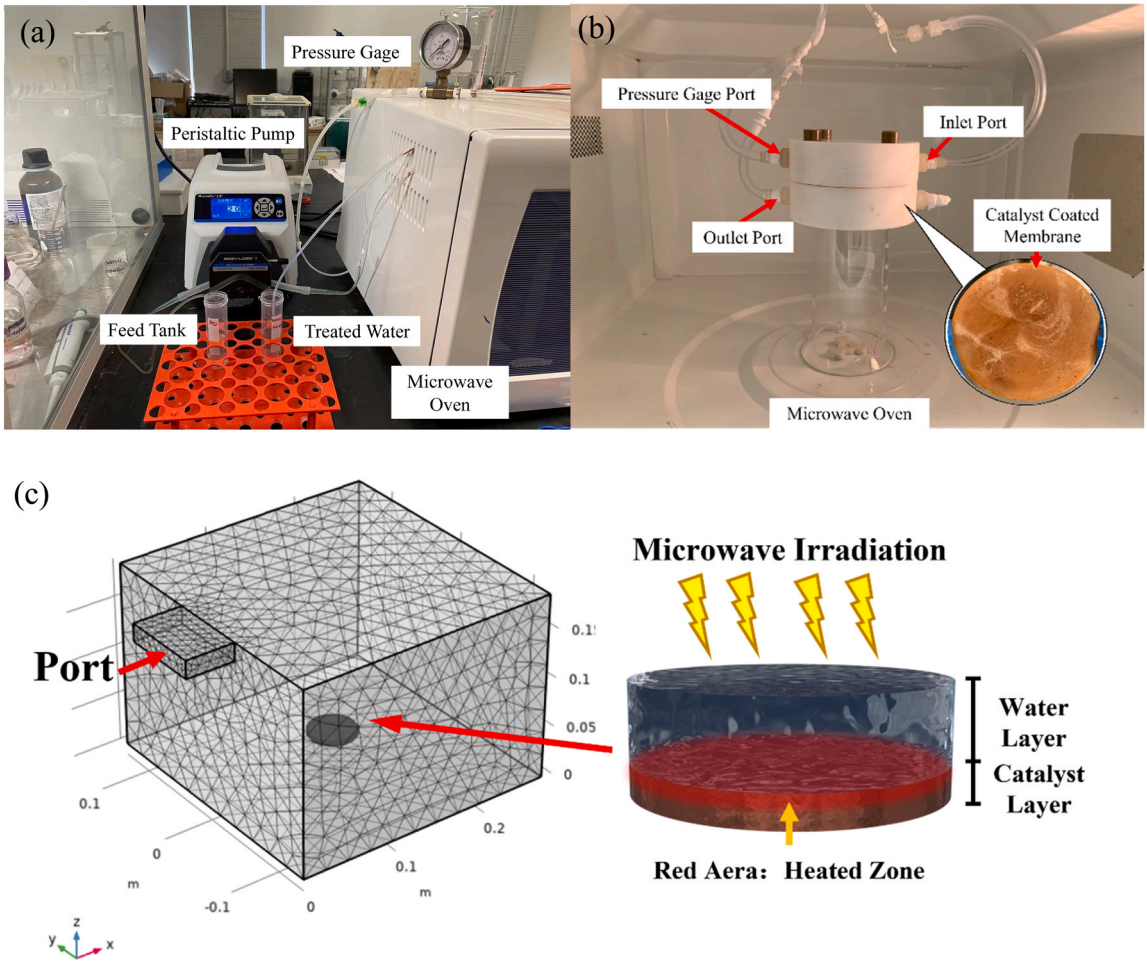

Fig. 1. (a) The MS2 suspension was pumped into the membrane filtration cell by a peristaltic pump. (b) The PTFE membrane filtration cell in the microwave oven. (c) The geometry of the microwave chamber, catalyst layer and water layer in COMSOL simulation.

(DMPO) as a scavenger. In this study, 8 mg BFO was mixed with 300 μL of 150 mM DMPO in DI water, transferred into a 50 μL glass capillary and then measured on a Bruker Magnettech ESR5000 using the following parameters: microwave frequency of 9.463 GHz; microwave power of 10 mW; field modulation width of 0.1 mT; and sweep time of 60 s. TiO_2 was chosen as a negative control and subjected to identical measurement conditions. ESR Studio Software was used to simulate the spectra and conduct quantitative analysis.

2.6. Analysis of interfacial heat distribution and microwave penetration

The heat distribution across the BFO catalyst layer was simulated using COMSOL Multiphysics (6.0). To simplify the simulation, the catalyst layer was assumed to be a thin sheet, and a phase change (e.g., melting) of the catalyst were ignored as described in S5.1. The simulations predicted the temperature changes of the interface between the water layer and the catalyst layer during microwave irradiation. They also predicted the microwave penetration depth with different water or catalyst thicknesses.

Fig. 1c shows the geometry of the microwave chamber and the catalyst and water layers. Detailed information on material parameters and dimension parameters are in Table S1-S2. Briefly, a Transition Boundary Condition (TBC) was used to define the thin catalyst layer (20 μm) in COMSOL's electromagnetic module, because TBC is appropriate for conductive materials with a layer thickness relatively smaller than the skin depth of the BFO (about 4.5 mm [44]) being modeled. Information on the COMSOL simulations, including model assumptions, electromagnetic field model, and heat transfer model, are provided in **Section S5**.

3. Results and discussion

3.1. Evaluation of MS2 inactivation in batch experiments

Fig. 2a compares the log reduction of MS2 for the batch experiments. Compared to the negative control, all treatments showed decent levels of MS2 reduction. For example, microwave irradiation and 70 °C water exposure achieved a similar MS2 reduction that was higher than that under the catalyst exposure without microwave exposure. As heating the water could have denatured viral biomolecules (e.g., viral capsid, RNA and proteins), the elevated temperatures (43–70 °C) apparently achieved similar MS2 inactivation due to microwave irradiation alone. In contrast, the removal of MS2 by BFO catalysts (no microwave irradiation) should primarily be attributed to surface adsorption. For example, a high adsorption capacity of MS2 (2.49×10^{11} PFU•g^{-1}) was reported on hematite (Fe_2O_3) nanoparticles (a similar metal oxide to BFO) via adsorption [45]. Most important is that the combination of microwave irradiation and catalyst led to the highest MS2 removal (0.66 log

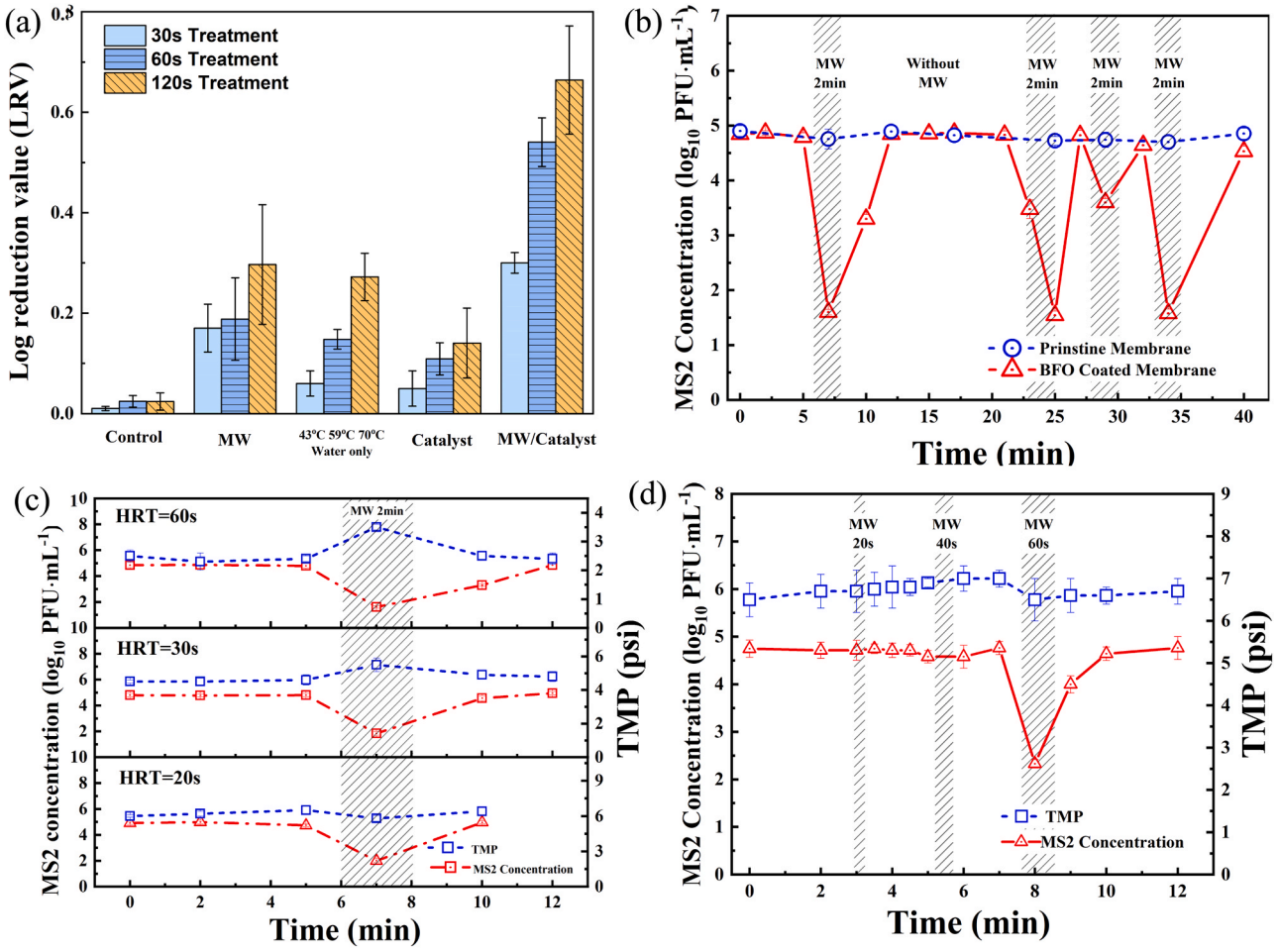

Fig. 2. (a) MS2 inactivation (LRV) for the different treatment conditions after 30 s, 60 s, and 120 s (b) MS2 concentration changes in four consecutive cycles of membrane filtration through the pristine and BFO coated membranes. The shaded bar indicates the operation of microwave irradiation during filtration, whereas other areas were operated without microwave irradiation; the irradiation time was 2 min; the permeate flux was 69 LMH and hydraulic retention time (HRT) was 60 s (c) The change of MS2 concentration and TMP at HRT of 60 s, 30 s and 20 s, respectively. irradiation time:2 min (d) The change of MS2 concentration and TMP with different irradiation time (20 s, 40 s and 60 s); the permeate flux: 207 LMH and HRT: 20 s other experimental conditions: the microwave intensity: 125 watts (7.2 watt·cm^{-2}), microwave frequency: 2.45 GHz.

removal or 76% in 120 s), because thermal and non-thermal effects, such as from ROS, contributed to MS2 removal [33,46]. Non-thermal effects and ROS generation are analyzed in the following sections.

3.2. MS2 inactivation in the microwave-assisted membrane filtration

Fig. 2b compares MS2 inactivation on a pristine (catalyst-free) membrane versus the membrane coated with BFO catalyst in continuous filtration with intermittent microwave irradiation. Without microwave irradiation, neither the pristine membrane nor the BFO-coated membrane yielded significant removal of MS2, which indicates that adsorption and size exclusion were negligible due to the small diameter of MS2 (27 nm) compared to the membrane's pore sizes (140 nm). In contrast, microwave irradiation for 2 min (marked by the shaded bar) yielded significant reductions in the MS2 concentration in the filtrate, especially with the catalyst-coated membrane. While the average LRV was 0.5 for the pristine membrane, the BFO-coated membrane achieved an LRV of 3.3, confirming the pronounced non-thermal effect on viral inactivation. The enhanced viral inactivation during microwave irradiation was observed in each of three subsequent cycles. Moreover, the LRV during BFO-coated membrane filtration with microwave irradiation (3.3) was much higher than the LRC in the batch experiment (0.66) with the BFO-coated catalyst. This enhancement can be attributed to improved mass transfer and virus-catalyst interactions in membrane filtration.

Fig. 2c shows the changes of the MS2 concentration in the filtrate and TMP for the permeate fluxes from 69 to 207 LMH, which correspond to hydraulic retention times (HRTs) of 60, 30, and 20 s, respectively. Without microwave irradiation, the removal of MS2 was not significantly affected by the permeate flux (LRV $=0.04 \pm 0.02$). With microwave irradiation turned on at the filtration time of 6 min, the MS2 concentrations at HRTs of 60, 30, and 20 s decreased appreciably, with the corresponding LRVs of 3.3, 2.7, and 2.6; this means that increasing HRT favored the MS2 removal. Furthermore, with 125-W microwave irradiation for 2 min, the TMP increased from 2.4 psi to 3.5 psi and from 4.5 psi to 5.5 psi for HRTs of 30 s and 60 s, respectively. However, the TMP decreased from 6.5 psi to 5.8 psi for an HRT of 20 s after 60-s microwave irradiation, probably because surface bubbling removed surface foulants within the membrane pores or on the membrane surface, which increased the water permeability and reduced TMP.

We compared the effects of irradiation time on MS2 removal using the same HRT of 20 s Fig. 2d shows that the MS2 concentration remained unchanged in the filtrate with microwave irradiation for 20 or 40 s but increasing the microwave irradiation time to 60 s increased the LRV to 2.6. Moreover, the TMP declined with 60-s microwave irradiation, probably due to a membrane defouling process and possibly reduced water surface tension at increased temperatures. When the microwave was off, the MS2 concentration resumed to the level in the feed, and the TMP level also increased to 5.5 psi.

Our previous study examined the stability of catalytic activity and dissolution potential of BFO catalyst during microwave catalytic filtration. The results showed that the BFO catalysts maintained high catalytic activity and had low metal leaching after five to six cycles of microwave-enhanced Fenton-like reactions for degradation of perfluorooctanoic acid (PFOA) and 1,4-dioxane.[32,36] Fig. S4, which shows the measured transmembrane pressure (TMP) and LRV of MS2, indicates that MS2 removal decreased with the LRV reduced from 3.0 ± 0.6–2.2 ± 0.3 over five consecutive filtration cycles. TMP increased by ~20% by the last filtration cycle, probably due to membrane fouling caused by the deposition of any residual culture medium substances and adsorbed viruses.

3.3. The roles of radical and catalyst on viral inactivation in microwave-assisted membrane filtration

To investigate the roles of the reactive species in MS2 inactivation, Fig. S2 shows that the addition of scavengers of the hydroxyl radical (•OH) and superoxide radical ($\bullet O^{2-}$) consistently reduced the LRV for three doses of catalysts. The inhibition effect was most significant for •OH radicals. Radical formation was largely attributed to the formation of hot spots and nanobubbles on catalysts that may collapse and release the mechanical waves and oxidative species [32]. In addition, the catalyst concentration slightly affected MS2 inactivation during microwave irradiation. A low catalyst concentration (0.2 $g \bullet L^{-1}$) yielded greater viral removal than a high catalyst concentration (0.5 $g \bullet L^{-1}$). A high particle concentration increased the solution turbidity and decreased microwave penetration, which reduced microwave utilization for radical production and viral inactivation [47]. Moreover, the catalyst particles at high concentrations may adsorb viruses and shield them from effective attacks of radicals or local heating. Furthermore, in comparison to the negative control (Fig. 3a), the EPR spectrum shown in Fig. 3b exhibited a distinctive 1:2:2:1 quartet signal of DMPO-OH adduct, which confirms the generation of •OH on BFO catalyst under microwave irradiation [48]. The presence of other peaks was probably C-centered radicals due to the impurity in the samples [49]. The time course of DMPO-OH generation is presented in Fig. 3c, where DMPO-OH production increased up to 3.9×10^{-7} $mol \bullet L^{-1}$ within 11 min and then decreased. This decline could be attributed to the agglomeration and precipitation of catalyst suspension, which may have affected the absorption of microwaves and the generation of radicals.

The morphological changes of MS2 were assessed to reveal the structural damage by the microwave catalytic membrane filtration. The TEM image of MS2 before treatment shows an intact round-shaped capsid (Fig. 3d), which is the typical morphology of an active MS2 virus [50,51]. After treatment, obvious morphological changes were the irregular fragments in Fig. 3e. The viral morphology changes verified the effectiveness of microwave catalytic system toward viral inactivation.

According to the presented results, the high inactivation efficiency for MS2 using $BiFeO_3$ can be attributed to the •OH radical generated by microwave irradiation. As illustrated in Equation S1 to S6, $BiFeO_3$ could be excited to generate electron-hole pairs under microwave irradiation; the valence band holes quickly reacted with H_2O, OH^- and other groups to form •OH radicals [52], which damage the genomic and protein capsid of MS2 [53–55]. In theory, the energy of a microwave quantum is insufficient to excite valence electron to transition into conduction band via photoelectric effect [56], due to the low microwave frequencies (300 GHz–300 MHz) and corresponding high microwave wavelengths (1 mm to 1 m), compared to the minimum excitation frequency (5.14×10^6 GHz) of $BiFeO_3$ (binding energy of 21.3 eV) and corresponding maximum electromagnetic wavelength (58.3 nm, as calculated by Equation S7 and S8). However, according to our presented results and previous reports [36,57,58], MW irradiation generates electron-hole pairs in $BiFeO_3$ through the dipolar polarization, conduction and interfacial polarization [56]. Dipolar polarization originates from intermolecular inertia and contributes to the majority of microwave heat energy. When a dipole is exposed to a high-frequency alternating electric field of the microwave, there is a time lag between the reversal of the dipole and the alternating shift of the electric field. The polar particles or molecules collide with the adjacent molecules or atoms during the rotation and transform microwave energy into local heating [59,60]. Conduction occurs when electrons move through the conductive material under the influence of electric and magnetic fields of microwave in opposite directions, causing oscillation and collisions that generate heat. Interfacial polarization is the combination of conduction and dipolar polarization. $BiFeO_3$ has a wide frequency range of reflection loss and large negative values of up to approximately −24 dB at 2.45 GHz; thus it can efficiently absorb microwave energy [61]. Accordingly, the electronic work function of $BiFeO_3$ could be decreased as the valence electron of $BiFeO_3$ is activated by the local heating to migrate into the conduction band, which consequently produce radicals such as •OH and $\bullet O^2$.

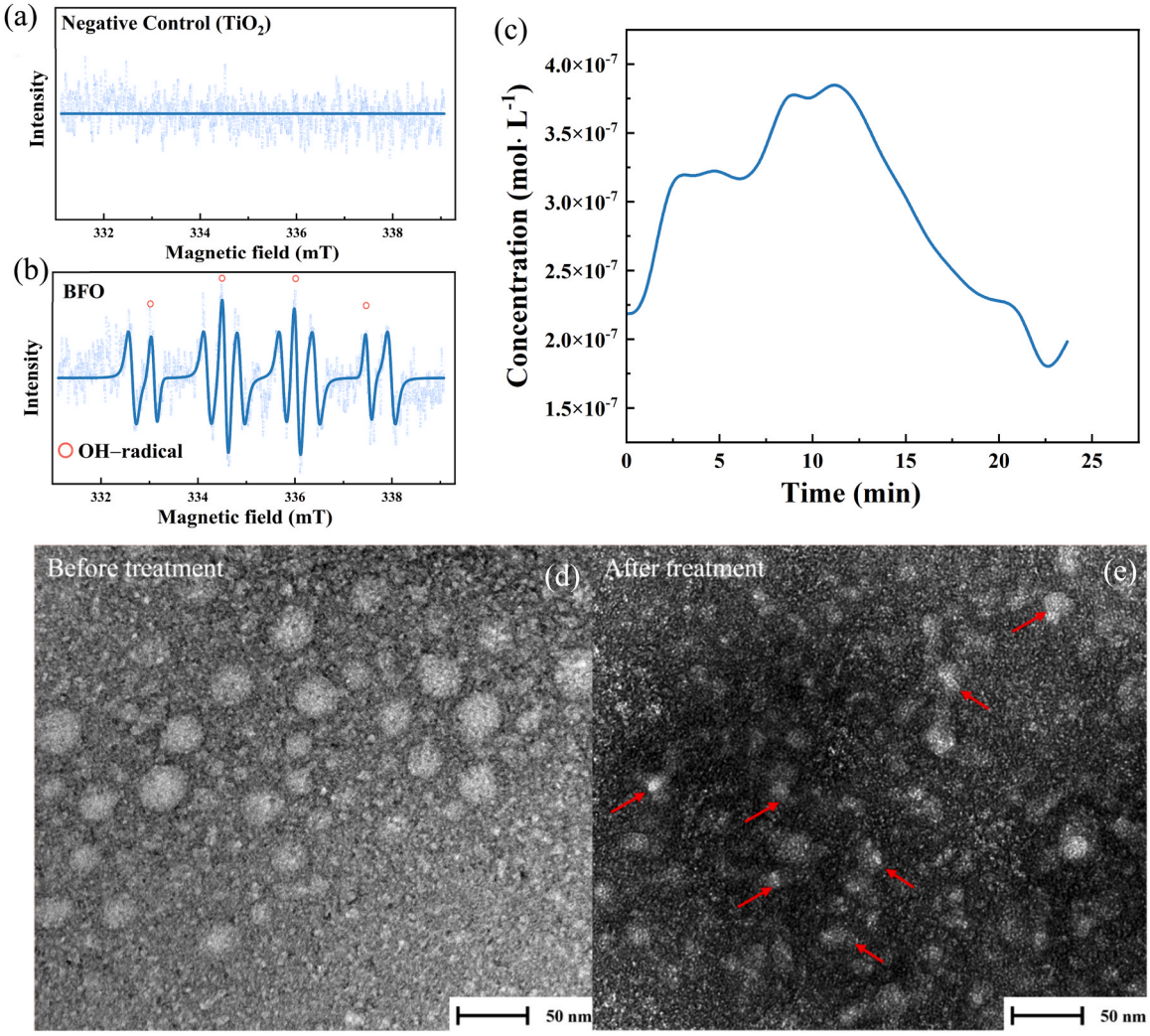

Fig. 3. EPR spectra generated in (a) a TiO_2 suspensions and (b) a BFO suspension include 150 mM DMPO under microwave irradiation (9.45 GHz, 10 mW); (c) the time course of DMPO-OH generation in the BFO suspension under microwave irradiation (9.45 GHz, 10 mW); TEM images of MS2 (d) before treatment and (e) after treatment by the microwave catalytic membrane filtration (the arrow shows the fragments of MS2).

3.4. Evaluation of microwave penetration across the catalyst and water layers

3.4.1. Microwave penetration of the BFO catalyst layer with different thickness

The inset of Fig. 4**a** shows a top view (x-y plane) and a cross-section view of the catalyst layer having a thickness of 1.6 mm in the microwave-oven chamber. The spatial distribution of temperature during microwave irradiation of 125 W and 2.45 GHz was simulated by COMSOL. A high-temperature (~400 °C) region is located at the central point, as marked by a red-hot spot, and low-temperature (blue) regions are at the edges. The center region is most intensely heated because the electromagnetic waves reflect off the catalyst and concentrate at the center point. The curves in Fig. 4**a** present the temperatures at the center of the catalyst layer decreases almost exponentially as the catalyst layer thickness increases from 2 μm to 12.6 mm with 2.45 GHz and 2 GHz, but the catalyst could not be heated due to the strong penetration ability of the low-frequency (0.45 GHz) microwave [62]. The temperature decline over the catalyst layer thickness matches well the exponential form of the microwave energy adsorption over the penetration depth in Eq. (2) [33,63].

$$p_{absx} = p_{abs0} \cdot e^{-2x/D_p} \quad (2)$$

where P_{abs0} and P_{absx} are the microwave power densities at the depth x (m) of the irradiated material (Watt·m^{-3}), respectively. D_p is the characteristic penetration depth of the microwave, which depends upon the relative dielectric permittivity of the microwave-absorbing materials and the microwave frequency [64–67].

3.4.2. Microwave penetration with different water thickness

Due to the strong absorption of microwave by water, the microwave penetration characteristics across a water film layer is critical to the rationale design of membrane filtration to ensure microwave energy utilization. To assess microwave penetration, the catalyst layer thickness was fixed at 2 μm with various water-layer thicknesses (i.e., 2–20 mm) above the catalyst layer. Fig. 4**b** shows that two symmetrical hot spots around y = ± 13 mm were created with temperatures of 150–305 °C generated at the interface of catalyst layer and water layer. The interfacial heating resulted from the reflection and refraction of microwave on the interface, which is also known as a standing wave effect [68]. The standing-wave effect occurs when two progressive waves of same amplitude and wavelength travel in opposite directions and superimpose [69]. The electromagnetic density of 820 V·m^{-1} was highest at the center of the interface, where the wavelengths overlap, which is why two symmetrical hot spots at the center of interface were observed in the four electromagnetic contour distribution in the inset of Fig. 4**b**. As the

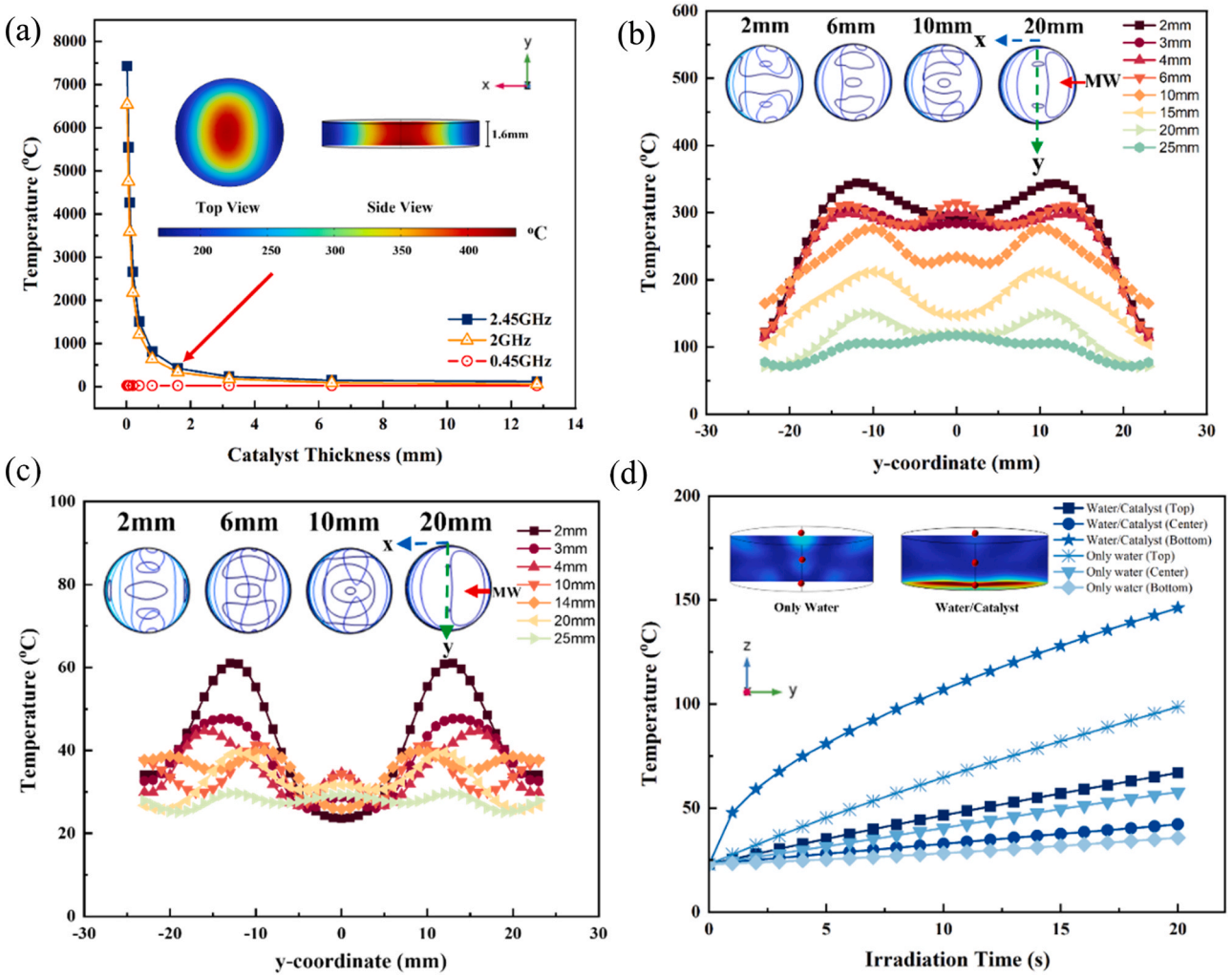

Fig. 4. (a) Temperature changes in the center of the catalyst layer as the catalyst thickness increases. The predicted temperature is located at the center point of the catalyst-coated round-shaped disk (23 mm in diameter) that is placed in a microwave oven chamber and irradiated by different microwave frequency. (b) The interfacial temperature profile of the catalyst surface along the y-coordinate at the different water layer thickness. (c) The interfacial temperature profile along the y-coordinate of the acrylic plastic surface (no microwave absorbing catalyst) at the different water layer thickness. (d) The thermodynamic analysis of the top, center and bottle points in a cross section of a 15-mm water layer with or without-catalyst. All simulation was performed under 125-W microwave irradiation for 20 s.

water-layer thickness increased from 6 mm to 10 mm, the standing wave phenomenon led to "oscillation" of the distribution of the electromagnetic field at the interface, which changed the temperature distribution with one more hot spots at center in Fig. 4**b** [68,70]. Moreover, Fig. S5 demonstrates that a water layer that is thicker than 10 mm could start to reflect and create additional heating zones within the water layer, and Fig. S6 indicates that the temperatures of the catalyst in a high electromagnetic field are significantly higher than in a weak electromagnetic field, while a close distance (<20 mm) to the microwave generator may cause over-heating on both sides of the catalyst. More discussions are provided in sections S5.7 and S5.8.

3.4.3. *Temperature profiles of the interfaces of catalyst and water*

To analyze the roles of the catalyst on microwave absorption and the water-layer temperature, we repeated the simulation of the interfacial temperature profile of the acrylic plastic surface (with no microwave absorption) along the y-coordinate that was covered by the water film of various thickness. Fig. 4**c** indicates that the interfacial temperature on the acrylic plastic surface wa significantly lower than that on the BFO catalyst surface (Fig. 4**b**). The inset in Fig. 4**c** shows that the electromagnetic distribution on the acrylic plastic surface was different in the presence of the BFO catalyst due to the changes in electromagnetic properties, particularly relative permittivity.

Fig. 4**d** compares the temperature increase of a water film of 15-mm thickness at top, center, and bottom positions and with or without the presence of the catalyst layer. The water layer at the bottom position in contact with the catalyst exhibited the fastest temperature increase and reached the highest temperature, near 150 °C (starred data points). However, the temperatures at the top and center positions of the water layer with catalysts were lower than those without catalysts, probably because the catalyst competed with water and consumed microwave energy. Fig. 4**d** compares the heat mapping of the water layer and illustrates that, without catalysts, several hot spots (light blue regions) were generated. However, with catalysts, the microwave energy selectively heated the catalysts and led to a lower water temperature.

3.5. *Assessment of Energy Efficiency*

Table S3 summarizes the energy source, retention time, and Electrical Energy per Order (E_{EO}) for different viral- and bacterial-disinfection processes. The energy consumption of microwave-assisted membrane filtration and photocatalytic membrane filtration are significantly lower than that of corresponding static experiments due to the enhanced mass transfer and specific surface area in membrane filtration

process. For example, we calculated E_{EO} values for microwave-assisted membrane filtration operated at relevant HRTs and irradiation time. Fig. S7 shows that HRTs of 20 with microwave irradiation yielded the lowest value of E_{EO} (189 $Wh \cdot m^{-3} \cdot order^{-1}$). Despite of its relatively high E_{EO} values for viral removal, microwave-enabled catalytic membrane filtration offers new added advantages such as efficient microwave penetration or energy dissipation (compared to UV irradiation), selective microwave adsorption, and reduced membrane fouling.

4. Conclusion

This study aimed to evaluate microwave-assisted membrane filtration in MS2 inactivation. Electromagnetic-wave energy was converted to local heat (e.g., 305 ^{o}C) and radicals on the BFO catalyst; both effects contribute to a log removal of up to 2.6 was achieved for MS2 within a contact time of 20 s using 125-W microwave irradiation. Hydraulic retention time (HRT), microwave irradiation time and microwave power were optimized, and stability of the coated membrane for MS2 inactivation under microwave irradiation system were examined. EPR measurement and radical scavenging experiments were conducted to confirm that hydroxyl radical is the key reactive species during microwave-catalytic viral inactivation. COMSOL simulation was employed to assess electromagnetic heating and penetration with varying catalyst thickness and water layer thickness. This technology holds great promise for point-of-use disinfection of water to supply safe drinking water or treat biohazardous wastewater generated in hospitals or pharmaceutical processes.

Environmental implications

Waterborne viruses like norovirus, rotavirus, adenovirus, and enterovirus pose a grave risk to public health and the environment due to their small size, strong pathogenicity, and resistance to disinfectants. This pioneering study presents a breakthrough solution through a novel microwave-enhanced membrane filtration process that generates localized heating and radicals to effectively inactivate waterborne viruses. This cutting-edge research has the potential to revolutionize water treatment strategies, safeguarding communities from gastrointestinal, respiratory, and neurological diseases caused by waterborne viruses. It offers a compelling solution to combat the persistent threat of waterborne viral illnesses, paving the way for a safer future.

CRediT authorship contribution statement

Fangzhou Liu: Conceptualization, Data curation, Formal analysis, Investigation, Methodology, Writing – original draft. **Bruce Rittmann**: Writing – review & editing. **Saachi Kuthari**: Methodology, Investigation and Writing – original draft. **Wen Zhang**: Writing – review & editing.

Declaration of Competing Interest

The authors declare that they have no known competing financial interests or personal relationships that could have appeared to influence the work reported in this paper.

Data availability

Data will be made available on request.

Acknowledgements

The authors gratefully acknowledge funding support from the United States Department of Interior via Bureau of Reclamation (Agreement number: R19AC00106), EPA P3 Phase I and II (SU84015001 and SV84041901), and NSF Molecular Separation (Award number: 2025374), and 2021–2022 NJIT's Undergraduate Research and Innovation (URI) Seed Grant and 2022 Summer Research Fellowship.

Supporting Information

Detailed information about characterization of the BFO catalyst-coated membrane and membrane filtration system (Section S1); The method of revival and propagation of MS2 (Section S2); roles of radical and catalyst on viral inactivation (Section S3); stability examine of coated membrane (Section S4); details associated with the simulation methodology, and model settings used in COMSOL (Section S5); comparison of electrical energy per order (E_{EO}) in irradiation-based disinfection and microwave assisted membrane filtration system in different experimental conditions (Section S6).

Appendix A. Supporting information

Supplementary data associated with this article can be found in the online version at doi:10.1016/j.jhazmat.2023.131966.

References

[1] Prado, T., de Castro Bruni, A., Barbosa, M.R.F., Garcia, S.C., de Jesus Melo, A.M., Sato, M.I.Z., 2019. Performance of wastewater reclamation systems in enteric virus removal. Sci Total Environ 678, 33–42.
[2] Schlindwein, A., Rigotto, C., Simões, C., Barardi, C., 2010. Detection of enteric viruses in sewage sludge and treated wastewater effluent. Water Sci Technol 61, 537–544.
[3] Antony, A., Blackbeard, J., Leslie, G., 2012. Removal efficiency and integrity monitoring techniques for virus removal by membrane processes. Crit Rev Environ Sci Technol 42, 891–933.
[4] Zhang, C., Li, Y., Shuai, D., Shen, Y., Wang, D., 2019. Progress and challenges in photocatalytic disinfection of waterborne viruses: a review to fill current knowledge gaps. Chem Eng J 355, 399–415.
[5] Quevedo, R., Bastías, J.M., Espinoza, T., Ronceros, B., Balic, I., Muñoz, O., 2020. Inactivation of Coronaviruses in food industry: the use of inorganic and organic disinfectants, ozone, and UV radiation. Sci Agropecu 11, 257–266.
[6] Tizaoui, C., 2020. Ozone: a potential oxidant for COVID-19 virus (SARS-CoV-2). Ozone Sci Eng 42, 378–385.
[7] Bayarri, B., Cruz-Alcalde, A., López-Vinent, N., Micó, M.M., Sans, C., 2021. Can ozone inactivate SARS-CoV-2? a review of mechanisms and performance on viruses. J Hazard Mater 415, 125658.
[8] Gall, A.M., Shisler, J.L., Mariñas, B.J., 2015. Analysis of the viral replication cycle of adenovirus serotype 2 after inactivation by free chlorine. Environ Sci Technol 49, 4584–4590.
[9] Sharma, V.K., Zboril, R., McDonald, T.J., 2014. Formation and toxicity of brominated disinfection byproducts during chlorination and chloramination of water: a review. J Environ Sci Health Part B 49, 212–228.
[10] U.S.E. (2011), Water treatment manual: disinfection, pp 200.
[11] Fukuhara, T., 2019. Endornaviruses: persistent dsRNA viruses with symbiotic properties in diverse eukaryotes. Virus Genes 55, 165–173.
[12] Atanasova, N.D., Dey, R., Scott, C., Li, Q., Pang, X.-L., Ashbolt, N.J., 2018. Persistence of infectious enterovirus within free-living amoebae–a novel waterborne risk pathway. Water Res 144, 204–214.
[13] Olive, M., Gan, C., Carratalà, A., Kohn, T., 2020. Control of waterborne human viruses by indigenous bacteria and protists is influenced by temperature, virus type, and microbial species. Appl Environ Microbiol 86, e01992–01919.
[14] Duek, A., Arkhangelsky, E., Krush, R., Brenner, A., Gitis, V., 2012. New and conventional pore size tests in virus-removing membranes. Water Res 46, 2505–2514.
[15] Gentile, G.J., Cruz, M.C., Rajal, V.B., de Cortalezzi, M.M.F., 2018. Electrostatic interactions in virus removal by ultrafiltration membranes. J Environ Chem Eng 6, 1314–1321.
[16] Goswami, K.P., Pugazhenthi, G., 2020. Credibility of polymeric and ceramic membrane filtration in the removal of bacteria and virus from water: a review. J Environ Manag 268, 110583.
[17] Cetlin, D., Pallansch, M., Fulton, C., Vyas, E., Shah, A., Sohka, T., et al., 2018. Use of a noninfectious surrogate to predict minute virus of mice removal during nanofiltration. Biotechnol Prog 34, 1213–1220.
[18] Singh, R., Bhadouria, R., Singh, P., Kumar, A., Pandey, S., Singh, V.K., 2020. Nanofiltration technology for removal of pathogens present in drinking water. In: Waterborne pathogens. Elsevier, pp. 463–489.
[19] Qiu, Y., Lee, B.E., Neumann, N., Ashbolt, N., Craik, S., Maal-Bared, R., et al., 2015. Assessment of human virus removal during municipal wastewater treatment in Edmonton, Canada. J Appl Microbiol 119, 1729–1739.
[20] Lu, R., Mosiman, D., Nguyen, T.H., 2013. Mechanisms of MS2 bacteriophage removal by fouled ultrafiltration membrane subjected to different cleaning methods. Environ Sci Technol 47, 13422–13429.
[21] Zhang, C., Li, Y., Li, J., 2020. Improved disinfection performance towards human adenoviruses using an efficient metal-free heterojunction in a vis-LED

photocatalytic membrane reactor: operation analysis and optimization. Chem Eng J 392, 123687.
[22] Habibi-Yangjeh, A., Asadzadeh-Khaneghah, S., Feizpoor, S., Rouhi, A., 2020. Review on heterogeneous photocatalytic disinfection of waterborne, airborne, and foodborne viruses: Can we win against pathogenic viruses. J Colloid Interface Sci 580, 503–514.
[23] Chen, M., Lei, Q., Ren, L., Li, J., Li, X., Wang, Z., 2021. Efficacy of electrochemical membrane bioreactor for virus removal from wastewater: performance and mechanisms. Bioresour Technol 330, 124946.
[24] Sun, M., Wang, X., Winter, L.R., Zhao, Y., Ma, W., Hedtke, T., et al., 2021. Electrified membranes for water treatment applications. ACS EST Eng 1, 725–752.
[25] Horovitz, I., Avisar, D., Luster, E., Lozzi, L., Luxbacher, T., Mamane, H., 2018. MS2 bacteriophage inactivation using a N-doped TiO2-coated photocatalytic membrane reactor: influence of water-quality parameters. Chem Eng J 354, 995–1006.
[26] Liang, S., Lin, H., Habteselassie, M., Huang, Q., 2018. Electrochemical inactivation of bacteria with a titanium sub-oxide reactive membrane. Water Res 145, 172–180.
[27] Ma, Q., Gao, J., Potts, C., Tong, X., Tao, Y., Zhang, W., 2022. Electrochemical aging and halogen oxides formation on multiwalled carbon nanotubes and Fe3O4@ g-C3N4 coated conductive membranes. Ind Eng Chem Res 61, 14260–14271.
[28] Bondino, F., Duman, S., Nappini, S., D'Olimpio, G., Ghica, C., Menteş, T.O., et al., 2022. Improving the efficiency of gallium telluride for photocatalysis, electrocatalysis, and chemical sensing through defects engineering and interfacing with its native oxide. Adv Funct Mater 32, 2205923.
[29] Deng, S., Zhang, G., Wang, X., Zheng, T., Wang, P., 2015. Preparation and performance of polyacrylonitrile fiber functionalized with iminodiacetic acid under microwave irradiation for adsorption of Cu (II) and Hg (II). Chem Eng J 276, 349–357.
[30] Kim, S.Y., Jo, E.K., Kim, H.J., Bai, K., Park, J.K., 2008. The effects of high-power microwaves on the ultrastructure of Bacillus subtilis. Lett Appl Microbiol 47, 35–40.
[31] Zhang, Y., Zhang, G., Wang, P., Wang, Q., 2017. Disinfection of municipal secondary effluents with microwave-induced electrodeless ultraviolet irradiation for water reuse. J Chem Technol Biotechnol 92, 1017–1025.
[32] Fu, W., Zhang, W., 2018. Microwave-enhanced membrane filtration for water treatment. J Membr Sci 568, 97–104.
[33] Liu, F., Hua, L., Zhang, W., 2020. Influences of microwave irradiation on performances of membrane filtration and catalytic degradation of perfluorooctanoic acid (PFOA). Environ Int 143, 105969.
[34] Kang, Y.-Q., Cao, M.-S., Yuan, J., Shi, X.-L., 2009. Microwave absorption properties of multiferroic BiFeO3 nanoparticles. Mater Lett 63, 1344–1346.
[35] Hong, Y., Li, J., Bai, H., Song, Z., Li, G., Wang, M., et al., 2020. Role of finite-size effect in BiFeO3 nanoparticles to enhance ferromagnetism and microwave absorption. Appl Phys Lett 116, 013103.
[36] Li, S., Zhang, G., Zhang, W., Zheng, H., Zhu, W., Sun, N., et al., 2017. Microwave enhanced Fenton-like process for degradation of perfluorooctanoic acid (PFOA) using Pb-BiFeO3/rGO as heterogeneous catalyst. Chem Eng J 326, 756–764.
[37] Dowd, S.E., Pillai, S.D., Wang, S., Corapcioglu, M.Y., 1998. Delineating the specific influence of virus isoelectric point and size on virus adsorption and transport through sandy soils. Appl Environ Microbiol 64, 405–410.
[38] Armanious, A., Aeppli, M., Jacak, R., Refardt, D., Sigstam, T., Kohn, T., et al., 2016. Viruses at solid–water interfaces: a systematic assessment of interactions driving adsorption. Environ Sci Technol 50, 732–743.
[39] Wu, X., Tang, A., Bi, X., Nguyen, T.H., Yuan, B., 2019. Influence of algal organic matter of microcystis aeruginosa on ferrate decay and MS2 bacteriophage inactivation. Chemosphere 236, 124727.
[40] Rafii, B., Tanswell, A.K., Otulakowski, G., Pitkänen, O., Belcastro-Taylor, R., O'Brodovich, H., 1998. O2-induced ENaC expression is associated with NF-κB activation and blocked by superoxide scavenger. Am J Physiol-Lung Cell Mol Physiol 275, L764–L770.
[41] Kapuge, T.K., Thalgaspitiya, W.R., Rathnayake, D., He, J., Kerns, P., Suib, S.L., 2020. Photo-generated reactive oxygen species assisted tandem amine homocoupling and amine-alcohol cross-coupling reaction on mesoporous spinel cobalt oxide. Appl Catal B: Environ 268, 118386.
[42] Song, K., Mohseni, M., Taghipour, F., 2019. Mechanisms investigation on bacterial inactivation through combinations of UV wavelengths. Water Res 163, 114875.
[43] Raeiszadeh, M., Taghipour, F., 2021. Inactivation of microorganisms by newly emerged microplasma UV lamps. Chem Eng J 413, 127490.
[44] Nadeem, M., Khan, W., Khan, S., Husain, S., 2020. Influence of Ni doping on the optical properties of BiFeO3 multiferroic. In: AIP Conference Proceedings. AIP Publishing LLC.
[45] Gutierrez, L., Li, X., Wang, J., Nangmenyi, G., Economy, J., Kuhlenschmidt, T.B., et al., 2009. Adsorption of rotavirus and bacteriophage MS2 using glass fiber coated with hematite nanoparticles. Water Res 43, 5198–5208.
[46] Zhang, A., Gu, Z., Chen, W., Li, Q., Jiang, G., 2018. Removal of refractory organic pollutants in reverse-osmosis concentrated leachate by Microwave–Fenton process. Environ Sci Pollut Res 25, 28907–28916.
[47] Zheng, X., Shen, Z.-p, Cheng, C., Shi, L., Cheng, R., Yuan, D.-h, 2018. Photocatalytic disinfection performance in virus and virus/bacteria system by Cu-TiO2 nanofibers under visible light. Environ Pollut 237, 452–459.
[48] Li, M., Chen, J., Wu, W., Wu, S., Xu, L., Dong, S., 2023. Diatomic Fe− Fe catalyst enhances the ability to degrade organic contaminants by nonradical peroxymonosulfate activation system. Nano Res 1–7.
[49] Dvoranová, D., Barbieriková, Z., Brezová, V., 2014. Radical intermediates in photoinduced reactions on TiO2 (an EPR spin trapping study). Molecules 19, 17279–17304.
[50] Kim, K., Narayanan, J., Sen, A., Chellam, S., 2021. Virus removal and inactivation mechanisms during iron electrocoagulation: capsid and genome damages and electro-fenton reactions. Environ Sci Technol 55, 13198–13208.
[51] Yang, C., Wen, L., Li, Y., Li, X.-y, 2022. Fabrication of SnO2-Sb reactive membrane electrodes for high-efficiency electrochemical inactivation of bacteria and viruses in water. Chem Eng J, 137327.
[52] Zhou, J., You, Z., Xu, W., Su, Z., Qiu, Y., Gao, L., et al., 2019. Microwave irradiation directly excites semiconductor catalyst to produce electric current or electron-holes pairs. Sci Rep 9, 5470.
[53] Rattanakul, S., Oguma, K., 2017. Analysis of hydroxyl radicals and inactivation mechanisms of bacteriophage MS2 in response to a simultaneous application of UV and chlorine. Environ Sci Technol 51, 455–462.
[54] Mayer, B.K., Yang, Y., Gerrity, D.W., Abbaszadegan, M., 2015. The impact of capsid proteins on virus removal and inactivation during water treatment processes. Microbiol Insights 8. MBI. S31441.
[55] Nieto-Juarez, J.I., Kohn, T., 2020. The metal catalyst influences the kinetics and mechanisms of MS2 inactivation in Fenton-like Systems. Chimia 74, 149-149.
[56] Qiu, Y., Zhou, J., 2019. Highly effective and green microwave catalytic oxidation degradation of nitrophenols over Bi2O2CO3 based composites without extra chemical additives. Chemosphere 214, 319–329.
[57] Qiu, Y., Zhou, J., Cai, J., Xu, W., You, Z., Yin, C., 2016. Highly efficient microwave catalytic oxidation degradation of p-nitrophenol over microwave catalyst of pristine α-Bi2O3. Chem Eng J 306, 667–675.
[58] Wei, R., Wang, P., Zhang, G., Wang, N., Zheng, T., 2020. Microwave-responsive catalysts for wastewater treatment: a review. Chem Eng J 382, 122781.
[59] Liu, X., Xu, D., Zhang, D., Zhang, G., Zhang, L., 2016. Superior performance of 3 D Co-Ni bimetallic oxides for catalytic degradation of organic dye: investigation on the effect of catalyst morphology and catalytic mechanism. Appl Catal B: Environ 186, 193–203.
[60] Remya, N., Lin, J.-G., 2011. Current status of microwave application in wastewater treatment-a review. Chem Eng J 166, 797–813.
[61] Li, Y., Sun, N., Liu, J., Hao, X., Du, J., Yang, H., et al., 2018. Multifunctional BiFeO3 composites: absorption attenuation dominated effective electromagnetic interference shielding and electromagnetic absorption induced by multiple dielectric and magnetic relaxations. Compos Sci Technol 159, 240–250.
[62] Tripathi, M., Sahu, J., Ganesan, P., Monash, P., Dey, T., 2015. Effect of microwave frequency on dielectric properties of oil palm shell (OPS) and OPS char synthesized by microwave pyrolysis of OPS. J Anal Appl Pyrolysis 112, 306–312.
[63] Nowak, D., 2017. The impact of microwave penetration depth on the process of heating the moulding sand with sodium silicate. Arch Foundry Eng 17, 115–118.
[64] Schmink, J.R., Leadbeater, N.E., 2010. Microwave heating as a tool for sustainable chemistry. Microwave heating as a tool for sustainable chemistry. CRC Press,, Boca Raton, FL, pp. 1–24.
[65] Kappe, C.O., 2004. Controlled microwave heating in modern organic synthesis. Angew Chem Int Ed 43, 6250–6284.
[66] de la Hoz, A., 2011. Microwave Heating as a Tool for Sustainable Chemistry. In: Nicholas, E. (Ed.), Leadbeater. Wiley Online Library.
[67] Nowak, D., 2017. The impact of microwave penetration depth on the process of heating the moulding sand with sodium silicate. Arch Foundry Eng.
[68] Cao, H., Fan, D., Jiao, X., Huang, J., Zhao, J., Yan, B., et al., 2019. Importance of thickness in electromagnetic properties and gel characteristics of surimi during microwave heating. J Food Eng 248, 80–88.
[69] E. Kim, Control the standing wave effect by increasing low frequency source power, in: APS Annual Gaseous Electronics Meeting Abstracts, (2018), pp. LW1. 056.
[70] Gao, X., Liu, X., Yan, P., Li, X., Li, H., 2019. Numerical analysis and optimization of the microwave inductive heating performance of water film. Int J Heat Mass Transf 139, 17–30.